JVST A
Journal of Vacuum Science & Technology A
ARTICLE
avs.scitation.org/journal/jva

Thermal atomic layer etching of VO_2 using sequential BCl_3 and SF_4 exposures: Observation of conversion, ligand-exchange, and oxidation state changes

Cite as: J. Vac. Sci. Technol. A **41**, 012603 (2023); doi: 10.1116/6.0002149
Submitted: 8 August 2022 · Accepted: 1 December 2022 ·
Published Online: 3 January 2023

View Online

Export Citation

CrossMark

Jonas C. Gertsch,[1] Jonathan L. Partridge,[1] Austin M. Cano,[1] Joel W. Clancey,[1] Victor M. Bright,[2] and Steven M. George[1]

AFFILIATIONS

[1]Department of Chemistry, University of Colorado, Boulder, Colorado 80309
[2]Department of Mechanical Engineering, University of Colorado, Boulder, Colorado 80309

Note: This paper is part of the 2023 Special Topic Collection on Atomic Layer Etching (ALE).

ABSTRACT

The thermal atomic layer etching (ALE) of VO_2 was demonstrated using sequential exposures of BCl_3 and SF_4. The VO_2 etch rate measured by quartz crystal microbalance investigations at 250 °C was 2.3 Å/cycle. The mass losses during individual BCl_3 and SF_4 reactions were nearly self-limiting versus BCl_3 and SF_4 exposures. The VO_2 etch rates were also dependent on temperature and varied from 0.05 Å/cycle at 150 °C to 2.3 Å/cycle at 250 °C. Fourier transform infrared (FTIR) spectroscopy studies observed VO_2 etching by monitoring the decrease in absorbance from V—O stretching vibrations in the VO_2 film. The FTIR spectra during the initial BCl_3 exposures on the VO_2 film observed the growth of absorbance from B—O stretching vibrations from B_2O_3 and the concurrent loss of V═O vibrational features. These changes were consistent with BCl_3 converting VO_2 to B_2O_3. The FTIR difference spectra during subsequent SF_4 and BCl_3 reactions also observed the growth and loss of absorbance features that were attributed to F_3V═O and V—F stretching vibrations, respectively. These changes indicate that SF_4 fluorinates VO_2 to form a VOF_3 surface layer and then BCl_3 undergoes ligand-exchange with VOF_3 to volatilize the VOF_3 surface layer as $VOCl_3$. There was also evidence for conversion of VO_2 to B_2O_3 during BCl_3 exposures and then removal of B_2O_3 by SF_4 exposures. In addition, quadrupole mass spectrometry (QMS) measurements observed that the SF_4 exposures produced ion intensities for $SO_xF_yCl_z$ products in oxidation states greater than 4+. These $SO_xF_yCl_z$ products indicate that SF_4 is being oxidized and acting as a deoxyfluorination reactant. Concurrently, the QMS analysis also monitored ion intensity for S_8^+, S_7^+, S_6^+, S_5^+, and S_4^+. These S_8 electron impact ionization products argue that SF_4 oxidation occurs concurrently with SF_4 reduction. The QMS also observed ion intensities corresponding to VCl_4^+ and $VOCl_3^+$. The presence of $VOCl_3^+$ indicates that the oxidation state of vanadium has increased to 5+ in some of the volatile etch products. The QMS also detected trichloroboroxin ($B_3O_3Cl_3$) during BCl_3 exposures. $B_3O_3Cl_3$ is a known etch product of B_2O_3 during BCl_3 exposures. BCl_3 can convert VO_2 to B_2O_3 and then proceed to etch the converted B_2O_3. Thermal VO_2 ALE using BCl_3 and SF_4 reveals the rich complexity of surface etching reactions that can proceed by multiple pathways including conversion, ligand-exchange, and oxidation state changes.

Published under an exclusive license by the AVS. https://doi.org/10.1116/6.0002149

I. INTRODUCTION

Atomic layer etching (ALE) is a highly controllable etch process that uses sequential and self-limiting surface reactions.[1,2] The first reaction typically modifies the surface. The second reaction then volatilizes the modified surface layer. ALE can be accomplished using either plasma or thermal methods.[1,2] Plasma ALE utilizes ions to remove the modified surface layer and can achieve directional anisotropic etching.[1] Plasma ALE has been demonstrated for numerous materials, such as Si,[3,4] SiO_2,[5] HfO_2,[6] Al_2O_3,[7] InP,[8] W,[9] graphene,[10] and MoS_2.[11] Thermal ALE uses molecular precursors to volatilize the modified surface layer and leads to conformal isotropic etching.[12,13] Thermal ALE has been reported for many materials including Al_2O_3,[13–17] HfO_2,[18–20] Ga_2O_3,[21] AlN,[22,23] TiN,[24] SiO_2,[25] Si,[26] W,[27] and Ni.[28]

Published under an exclusive license by the AVS

Various mechanisms have been reported for thermal ALE.[12] Many metal oxides and metal nitrides have been shown to undergo thermal ALE based on the fluorination and ligand-exchange mechanism.[12,17,29] The thermal ALE of other metal oxides is based on the initial conversion of the oxide surface to a different material followed by the removal of the conversion layer.[12,27] Elemental metals are also known to undergo thermal ALE based on initial oxidation or chlorination to change the initial oxidation state of the metal.[12,28,30] The oxidized metal can then be volatilized based on ligand-substitution or ligand-addition reactions.[28,30]

BCl_3 is a versatile reactant that can undergo ligand-exchange with metal fluorides to volatilize the metal fluoride by producing metal chlorides. BCl_3 was employed as a ligand-exchange precursor during AlN ALE using HF or XeF_2 for fluorination and BCl_3 for ligand-exchange.[22] BCl_3 was also employed as a ligand-exchange precursor during GaN ALE using XeF_2 for fluorination and BCl_3 for ligand-exchange.[31] In addition, BCl_3 has been utilized as a ligand-exchange precursor during TiO_2 ALE using WF_6 for fluorination and BCl_3 for ligand-exchange.[32]

BCl_3 is also able to convert the surface of many metal oxides to a B_2O_3 layer. This conversion reaction is thermodynamically favorable because B_2O_3 is more stable than many other metal oxides. The B_2O_3 conversion layer can then be spontaneously etched by HF to produce BF_3 and H_2O.[33] BCl_3 was used to convert WO_3 to B_2O_3 during WO_3 ALE.[27] B_2O_3 was then removed by spontaneous etching resulting from HF exposures. Recent results for Al_2O_3 ALE using BCl_3 and HF also revealed that Al_2O_3 ALE occurred by both fluorination and ligand-exchange together with conversion and spontaneous etching.[14]

In this paper, BCl_3 is demonstrated as a precursor for thermal VO_2 ALE together with SF_4 as the fluorination reactant. Earlier studies of VO_2 ALE utilized SF_4 for fluorination and $Sn(acac)_2$ for ligand-exchange.[34] SF_4 is a stronger fluorination reactant than HF. SF_4 was initially thought to be necessary for VO_2 fluorination because the ΔG^0 value for VO_2 fluorination to VF_4 using HF is positive.[34] However, experiments revealed that both SF_4 and HF could fluorinate VO_2 and subsequently etch the VO_2 film using $Sn(acac)_2$ as the ligand-exchange precursor.[34] Etch rates of 0.30 and 0.11 Å/cycle were measured for VO_2 ALE at 200 °C using SF_4 and HF, respectively, together with $Sn(acac)_2$.[34]

Because $Sn(acac)_2$ has low vapor pressure and poor thermal stability, the use of other ligand-exchange precursors for VO_2 ALE is desirable. BCl_3 has high vapor pressure and good thermal stability. However, BCl_3 has the possible complication of converting VO_2 to B_2O_3. The conversion reaction of VO_2 to B_2O_3 is as follows:

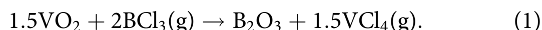

$$1.5VO_2 + 2BCl_3(g) \rightarrow B_2O_3 + 1.5VCl_4(g). \quad (1)$$

This reaction is thermochemically favorable with a standard free energy change of $\Delta G^0 = -37.5$ kcal/mol at 250 °C.[35] Consequently, the BCl_3 reaction during VO_2 ALE could lead to either ligand-exchange or conversion.

VO_2 is a technologically important material. VO_2 is a semiconductor at room temperature and has a metal–insulator transition around 68 °C that leads to a pronounced change in resistivity and optical transmittance.[36,37] As a result, VO_2 is useful for many devices, such as bolometers[38] and smart windows.[37,39] Thermal VO_2 ALE may be important to obtain thin VO_2 films with low thermal mass for sensitive thermal sensors. Thin VO_2 films are also less susceptible to fracture resulting from temperature cycling through the metal–insulator transition. High-quality, ultrathin, and continuous VO_2 films could be fabricated using VO_2 deposition followed by VO_2 etchback to overcome the problems of VO_2 nucleation on the underlying substrate.[40]

II. EXPERIMENT

A. Reaction conditions for VO_2 ALD and VO_2 ALE

The VO_2 films were deposited and etched in a custom-built, stainless-steel, viscous-flow reactor.[34] A total N_2 flow of 160 SCCM was used as both a purge and inert carrier gas. The reactor pressure was ∼1 Torr. The chamber was equipped with an *in situ* quartz crystal microbalance (QCM). An SC-cut quartz crystal (Maxtek SC-101 gold coated, 6 MHz) was used to monitor film growth and etch. A description of the reactor and QCM setup has been presented earlier.[34]

Vanadium (IV) oxide (VO_2) films were deposited in an ALD process at 150 °C using tetrakis(ethylmethylamino) vanadium(IV) (TEMAV, 98%, STREM) and DI H_2O as reactants.[34,41] The H_2O was kept at room temperature. The stainless-steel bubbler containing the TEMAV was heated to 60–65 °C and also used a N_2 flow-over of ∼20 SCCM to increase precursor transport into the reactor chamber. TEMAV and H_2O yield amorphous VO_2 ALD films when deposited at 150 °C.[41,42] As-deposited films were previously characterized to confirm VO_2 with a vanadium oxidation state of primarily 4+ using x-ray photoelectron spectroscopy (XPS).[34]

The VO_2 ALD films were then etched using boron trichloride (BCl_3, 99.9%, Sigma-Aldrich) and sulfur tetrafluoride (SF_4, >98.5%, SynQuest Laboratories). The VO_2 ALE was conducted at temperatures ranging from 150 to 250 °C. Both etching precursors were kept at room temperature. The pressures during BCl_3 and SF_4 exposures were 200 and 500 mTorr, respectively.

B. Reactor for *in situ* Fourier transform infrared spectroscopy measurements

VO_2 ALE was also studied using *in situ* Fourier transform infrared (FTIR) spectroscopy. The reactor and *in situ* FTIR spectrometer have been described previously.[43] The FTIR experiments employed high surface area silicon nanoparticles (>98%, U.S. Research Nanomaterials) with an average diameter of 30–50 nm. The Si nanoparticles were mechanically pressed into a tungsten grid support to facilitate the transmission FTIR measurements.[43] VO_2 ALD films were grown on the Si nanoparticles.

The tungsten grid was 2×3 cm^2, 50 μm thick, with 100 grid lines per inch. The tungsten grid was resistively heated using a DC power supply (6268B, 20 V/ 40 A, Hewlett-Packard). The voltage output of the power supply was controlled by a PID temperature controller (Love Controls 16B, Dwyer Instruments). A K-type thermocouple was attached at the bottom of the tungsten grid with epoxy (Ceramabond 571, Aremco). The epoxy also electrically isolated the thermocouple from the tungsten grid.

Published under an exclusive license by the AVS

C. Quadrupole mass spectrometry

Quadrupole mass spectrometry (QMS) was performed in a previously described reactor.[44] In this reactor, a mixture of N_2 carrier gas and precursor gas was used to form a molecular beam. This molecular beam was defined by gas expansion through an aperture on the sample chamber into vacuum. The beam then passed through a skimmer. The skimmer aperture diameter was 300 μm. The skimmer was positioned 33.4 mm from the sample aperture.

The beam then traveled into a differentially pumped region for the QMS analysis. Each QMS spectrum monitored mass intensities from 2 to 300 amu and had a 1 s scan time. An average of 20 scans was used to maximize the signal to noise in the spectra. An electron ionization energy of 70 eV was used for these experiments.

The QMS experiments were conducted on VO_2 and V_2O_5 powders placed in the sample holder. The powders were vanadium (IV) oxide (VO_2, >99% trace metals basis, Sigma-Aldrich) and vanadium (V) oxide (V_2O_5, >99% trace metals basis, Sigma-Aldrich). The mass of the VO_2 and V_2O_5 powders was measured before and after the etching experiments.

The QMS experiments were performed at 250 °C with a background N_2 pressure of 3.3 Torr defined by a N_2 flow of 2.0 SCCM through the sample chamber. Both BCl_3 and SF_4 were added to separate reservoirs to obtain a pressure of 8.0 Torr. During BCl_3 and SF_4 exposures, the BCl_3 and SF_4 reactants were added to the sample chamber. Each gas precursor dose was 120 s long, with 300 s purges between doses. During the BCl_3 and SF_4 exposures, the pressure in the sample chamber rose to 6.8 Torr. A partial pressure of 3.5 Torr was used for each precursor gas.

D. Transmission electron microscopy

Ex situ analysis of VO_2 film thickness and uniformity on particles before and after VO_2 ALE was performed using an FEI Tecnai T12, 20–120 V transmission electron microscope (TEM). The TEM was operated at 100 kV in the bright-field mode. W/WO_3 powder was chosen as the substrate material to provide enhanced contrast between the VO_2 ALD film and the substrate.

The VO_2 films to be analyzed with TEM were deposited at 150 °C using VO_2 ALD with TEMAV and H_2O as the reactants.[34,41] The VO_2 ALD films were etched at 250 °C using VO_2 ALE with BCl_3 and SF_4 as the reactants. This VO_2 ALE process was performed using static exposures in a separate reaction chamber that has been described previously.[45] The TEM samples were prepared by placing the VO_2 ALD-coated tungsten powder on a formvar/carbon-coated copper TEM grid (300 mesh, Electron Microscopy Sciences).

III. RESULTS AND DISCUSSION

A. QCM studies

VO_2 ALD films were first grown on the QCM sensor. The VO_2 ALD films were then etched using VO_2 ALE. Figure 1 shows QCM data of 115 cycles of VO_2 ALE using BCl_3 and SF_4 at 250 °C with BCl_3 exposures of 10 s and SF_4 exposures of 2.5 s. N_2 purge times were 90 s after BCl_3 doses and 135 s after SF_4 doses. This reaction sequence is designated as 10–90–2.5–135.

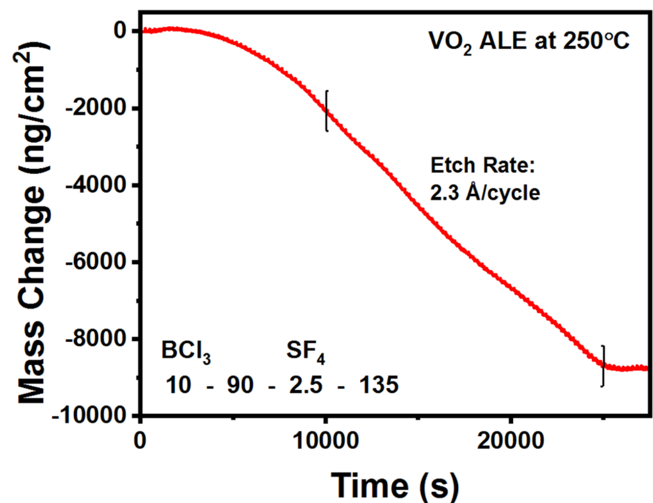

FIG. 1. Mass change vs time for 115 VO_2 ALE cycles using sequential BCl_3 and SF_4 exposures at 250 °C. Mass change per cycle yields an etch rate of 2.3 Å/cycle during the linear region designated by brackets.

An initial etch delay was observed with very slow etching during the first ∼30 cycles. This etch delay is not well understood at this time. The etch delay may result from a slow oxidation state change from V^{4+} to V^{5+} for vanadium surface species during initial BCl_3 and SF_4 exposures. Etching of V^{5+} species may be preferred as discussed later. After the delay, a linear etch regime is reached, and the average mass change per cycle (MCPC) is -101.2 ng/(cm^2 cycle). Assuming a VO_2 density of 4.36 g/cm^3 as measured by x-ray reflectivity (XRR), this MCPC corresponds to an etch rate of

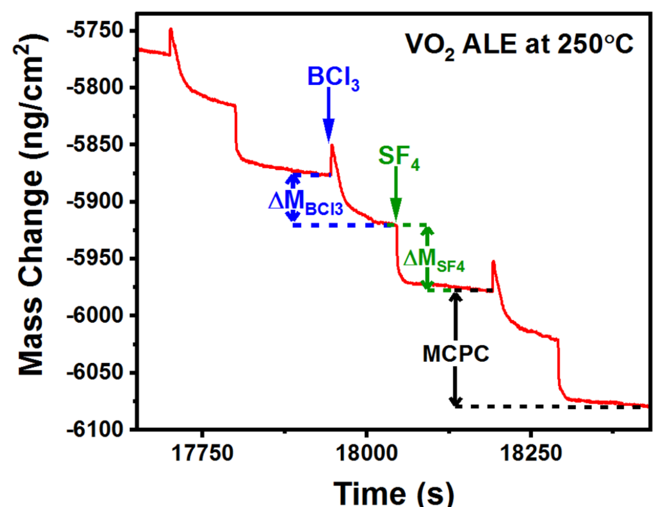

FIG. 2. Expanded view of three VO_2 ALE cycles from Fig. 2 in the linear region showing mass loss during both BCl_3 and SF_4 exposures.

Published under an exclusive license by the AVS

2.3 Å/cycle. No etching occurs during the last several cycles as shown in Fig. 2 because the initial VO_2 ALD film has been removed completely from the QCM sensor.

An expanded view of three VO_2 ALE cycles at 250 °C from the linear regime in Fig. 1 is shown in Fig. 2. The BCl_3 exposure leads to a mass loss of $\Delta M_{BCl3} = -44.3\ ng/cm^2$. The mass spike observed at the beginning of BCl_3 exposures may be attributed to initial BCl_3 adsorption on the surface that then undergoes ligand-exchange to produce volatile $VOCl_3$. Further mass loss occurs as extended BCl_3 exposure converts the underlying VO_2 surface to B_2O_3. Chlorinated species, such as BO_xCl_y, are also expected to remain on the surface after the BCl_3 exposure.

The SF_4 exposure leads to another mass loss of $\Delta M_{SF4} = -56.9\ ng/cm^2$. This mass loss is attributed to the removal of BO_xCl_y and B_2O_3 surface layers. Fluorination of the underlying VO_2 then forms a VOF_3 surface. During this fluorination, the vanadium is oxidized from a 4+ to a 5+ oxidation state. Sulfur is also believed to be reduced during this oxidation process.

Figure 3 explores the self-limiting nature of BCl_3 and SF_4 reactions at 250 °C. Each point represents the average mass change over 15 reaction cycles. In Fig. 3(a), the SF_4 exposure time was held constant at 2.5 s as the BCl_3 exposure time was varied from 0 to 20 s. The reactant pulse sequence is designated as X–90–2.5–135. The BCl_3 exposure exhibits a soft saturation behavior, where the mass change per cycle (MCPC) continues to decrease slightly with increasing exposure time. This slow decrease is likely due to slow spontaneous etching of the newly formed B_2O_3 surface by BCl_3 that forms volatile $B_3O_3Cl_3$ species.

In Fig. 3(b), the BCl_3 exposure was held constant at 10 s as the SF_4 exposure was varied from 0 to 5 s. This reactant pulse sequence is designated as 10–90–X–135. Figure 3(b) shows that the mass change per cycle decreases rapidly versus the SF_4 exposure. Saturation behavior is reached more quickly than for the BCl_3 exposure observed in Fig. 3(a). The SF_4 can readily remove the converted B_2O_3 surface layer and fluorinate the VO_2 surface.

The temperature dependence of VO_2 ALE is explored in Fig. 4. The temperatures ranged from 150 to 250 °C. The etch rates increased at higher temperatures. The etch rates were 0.05, 0.15, 0.20, 1.7, and 2.3 Å/cycle at 150, 175, 200, 225, and 250 °C, respectively. Using an Arrhenius plot to calculate an activation energy from the temperature-dependent linear etch regimes yields $E_a = 74.0\ kJ/mol$. An etch delay was observed at temperatures

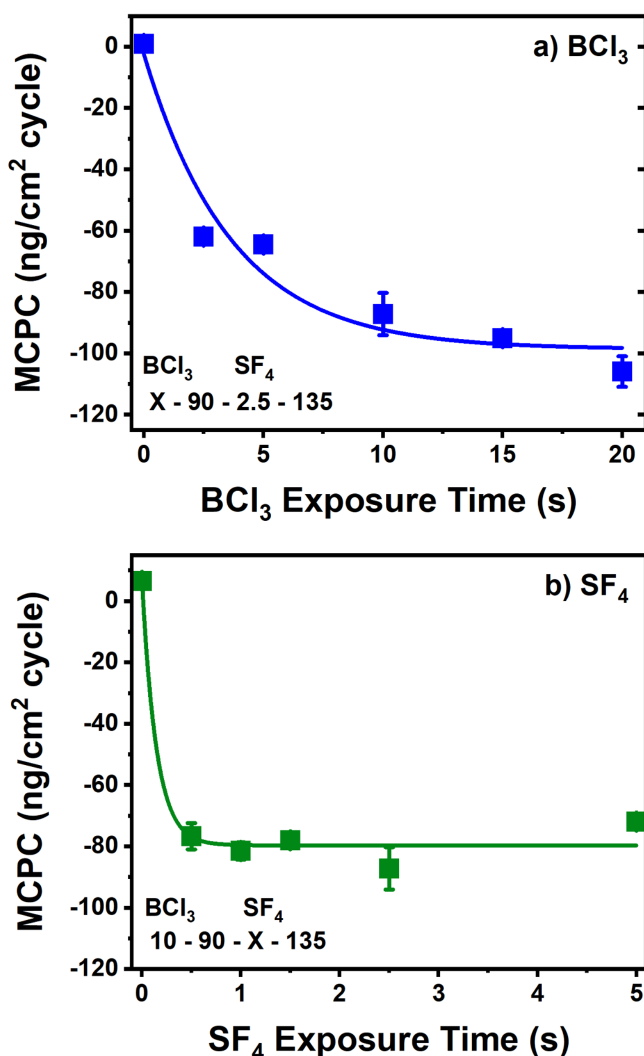

FIG. 3. Mass change per cycle (MCPC) vs exposure time during VO_2 ALE at 250 °C. (a) Varying exposure time, X, of BCl_3 with constant SF_4 exposure time of 2.5 s. (b) Varying exposure time, X, of SF_4 with constant BCl_3 exposure time of 10 s. Purge times were 90 and 135 s after BCl_3 and SF_4 exposures, respectively.

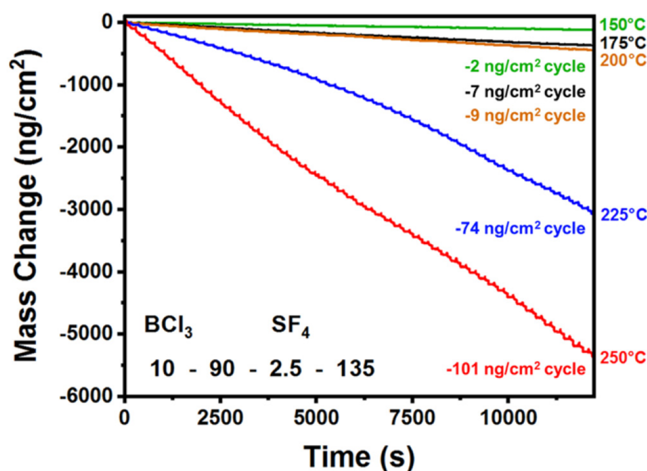

FIG. 4. Mass change vs time for VO_2 ALE using sequential BCl_3 and SF_4 exposures showing temperature dependence. Etch rates varied from 0.05 Å/cycle at 150 °C to 2.3 Å/cycle at 250 °C. Initial etch delays at 225 and 250 °C were removed to allow for better comparison between temperatures.

Published under an exclusive license by the AVS

>200 °C. These initial etch delays are not shown for 225 or 250 °C to allow for better comparisons. The etch delays were ~6000 s (25 etch cycles) and ~7000 s (30 etch cycles) for etching at 225 and 250 °C, respectively.

B. FTIR studies

Absolute infrared absorbance spectra showing the loss of absorbance of V—O stretching vibration from VO_2 are displayed in Fig. 5. Spectra are shown for 30 VO_2 ALE cycles using BCl_3 and SF_4 as the reactants at 250 °C. The black line indicates the spectrum for the as-deposited VO_2 ALD film referenced to the FTIR spectrum of the Si nanoparticle substrate. Spectra were recorded after every 5 VO_2 ALE cycles following the SF_4 exposures. The spectra are also referenced to the spectrum of the Si nanoparticle substrate.

The decreasing absorbance in the region of 400–850 cm^{-1} in Fig. 5 during VO_2 ALE is consistent with a loss of V—O stretching vibrations.[46,47] The absorbance loss from 980 to 1055 cm^{-1} during VO_2 ALE is attributed to V═O surface vibrations.[46,47] The initial increase in absorbance during first several etching cycles can be explained by the creation of vanadium fluoride stretching vibrations.[48,49] A decrease in absorbance is also observed at 925 cm^{-1} and is attributed to the loss of Si—O—V vibrations.[50] The Si—O vibration observed at 1215 cm^{-1} is due to oxidation of the underlying Si nanoparticle substrate during the VO_2 ALD growth.

Figure 6 explores initial BCl_3 exposures on a newly grown VO_2 ALD surface at 250 °C. The FTIR spectra show the result of eight BCl_3 exposures for 1 s. Progressive exposures are indicated by an increasing line darkness between the individual spectra. Figure 6 shows that there is a pronounced increase in absorbance at 1350 cm^{-1}. This absorbance is assigned to a B—O stretching vibration.[51] This increase in absorbance is attributed to the conversion of the surface of the VO_2 ALD film to a B_2O_3 surface layer.

There is also a distinct loss of absorbance at 1016 cm^{-1} in Fig. 6. This feature is assigned to a V═O surface species that is removed during the conversion of VO_2 to B_2O_3.[46,47] The growth of absorbance for the B–O stretching vibration and loss of absorbance for the V═O surface species is consistent with the conversion of VO_2 to B_2O_3 by BCl_3 according to the reaction given in Eq. (1). Some of the additional absorbance peaks in Fig. 6 below 1000 cm^{-1} can be attributed to B—Cl vibrations.[52]

FTIR difference spectra in the steady-state regime during the 20th cycle of sequential BCl_3 and SF_4 exposures during VO_2 ALE are shown in Fig. 7. The difference spectra recorded after BCl_3 and SF_4 exposures were referenced to spectra after previous SF_4 and BCl_3 exposures, respectively. The large increases in absorbance at 1051 and 650 cm^{-1} in Fig. 7(a) are attributed to $F_3V{=}O$ and V—F stretching vibrations.[48,49] These vibrational features are formed by the fluorination of VO_2 during SF_4 exposures. Figure 7(b) shows that these vibrational features are removed during subsequent BCl_3 exposure.

Small absorbance changes in the region of B—O stretching vibration around 1350 cm^{-1} are also observed in Fig. 7 during VO_2 ALE. A small peak corresponding to a B—O stretching vibration is observed in Fig. 7(b) after BCl_3 exposures. This slight peak is then removed in Fig. 7(a) during the subsequent SF_4 exposure. Similar behavior was also observed during Al_2O_3 ALE using BCl_3 and HF as reactants.[14] The BCl_3 exposures were also converting Al_2O_3 to B_2O_3. The HF exposures then spontaneously removed the B_2O_3 conversion layer.[33]

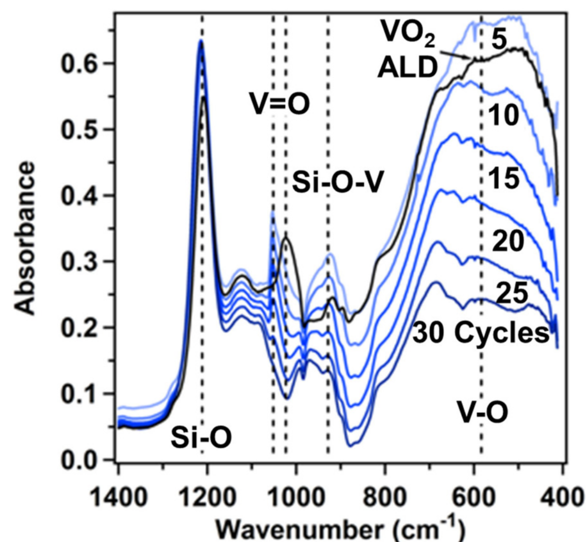

FIG. 5. Absolute FTIR absorbance spectra showing loss of V—O stretching vibrations during 30 cycles of VO_2 ALE using sequential BCl_3 and SF_4 exposures at 250 °C. Initial FTIR spectrum of the VO_2 ALD film is referenced to initial Si nanoparticles and given by the black spectrum.

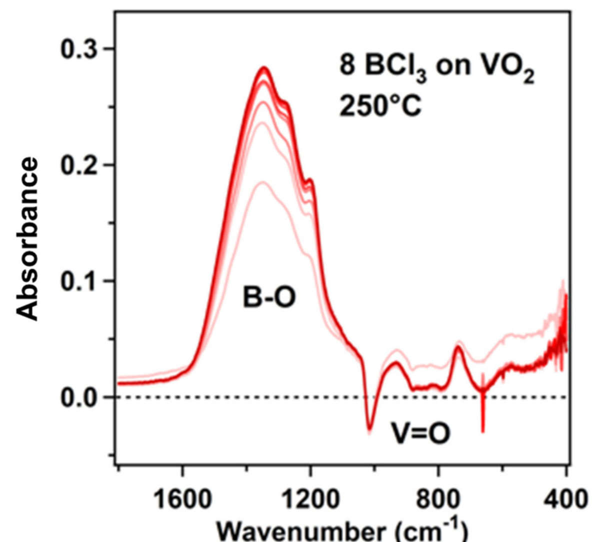

FIG. 6. Absolute FTIR absorbance spectra showing growth of B—O stretching vibrations and loss of V═O stretching vibrations during eight successive BCl_3 exposures on the initial VO_2 ALD film at 250 °C.

Published under an exclusive license by the AVS

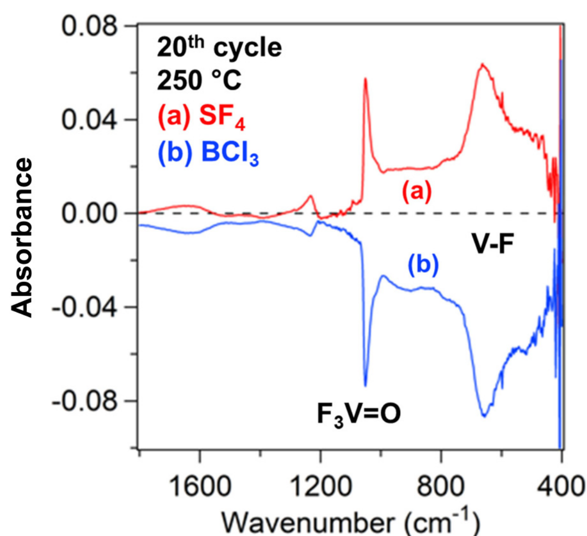

FIG. 7. FTIR difference spectra for 20th cycle of sequential BCl_3 and SF_4 exposures at 250 °C. (a) Difference spectrum after SF_4 exposure defined by referencing spectrum to spectrum after previous BCl_3 exposure. (b) Difference spectrum after BCl_3 exposure defined by referencing spectrum to spectrum after previous SF_4 exposure.

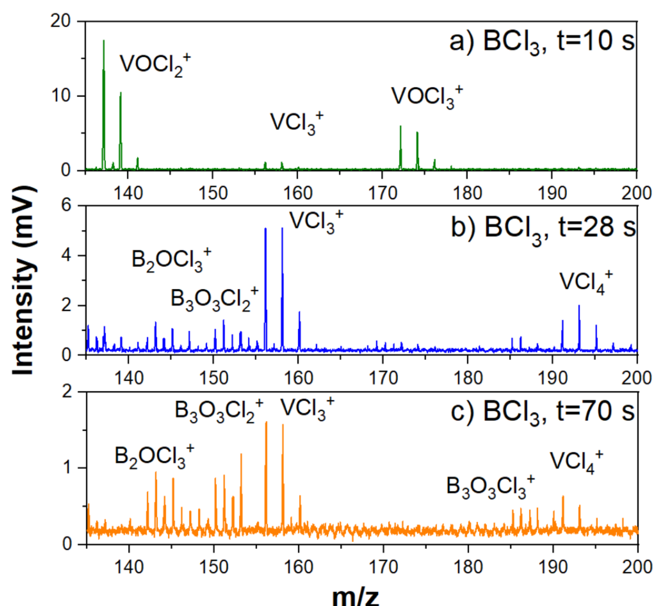

FIG. 9. QMS spectra recorded for third BCl_3 exposure during sequential BCl_3 and SF_4 exposures on V_2O_5 powder at 250 °C after exposure times of (a) 10, (b) 28, and (c) 70 s.

The absorbance increase for the B—O stretching vibration in Fig. 6 after BCl_3 exposure on a freshly deposited VO_2 ALD surface is much larger than the absorbance increase for the B—O stretching vibration in Fig. 7 after BCl_3 exposure during sequential SF_4 and BCl_3 exposures. This contrast is attributed to the difference between the two VO_2 surfaces. The VO_2 surface in Fig. 6 is the initial surface after VO_2 ALD. The VO_2 surface in Fig. 7 has been fluorinated by SF_4. The differences between Figs. 6 and 7 indicate that BCl_3 is not as effective converting the fluorinated VO_2 surface to B_2O_3.

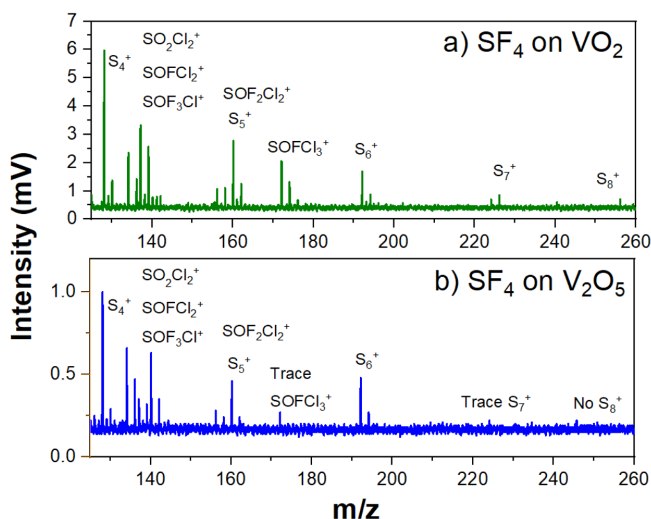

FIG. 8. QMS spectra recorded for 6th SF_4 exposure during sequential BCl_3 and SF_4 exposures on (a) VO_2 powder and (b) V_2O_5 powder at 250 °C.

C. QMS studies

QMS measurements at 250 °C for the 6th SF_4 exposure during sequential exposures of SF_4 and BCl_3 are shown in Fig. 8(a) for VO_2 powder and in Fig. 8(b) for V_2O_5 powder. The mass spectra cover m/z values from 110 to 260. Both oxidized and reduced sulfur species are observed compared with the parent SF_4 reactant. A variety of ion intensities are detected for $SO_xF_yCl_z$ products in oxidation states greater than 4+. These $SO_xF_yCl_z$ products indicate that SF_4 is being oxidized and acting as a deoxyfluorination reactant.

Ion intensities are also detected for S_8^+ and its electron impact cracking fragments including ion intensities for S_7^+, S_6^+, S_5^+, and S_4^+. These species are consistent with the reduction in the SF_4 reactant. A comparison of Figs. 8(a) and 8(b) reveals that the ion intensities for S_8 products are more intense on the VO_2 surface. The reduction in the SF_4 reactant is believed to coincide with the need for vanadium in VO_2 to oxidize from 4+ to 5+. This oxidization is required to produce stable volatile vanadium etch products in the 5+ oxidation state, such as $VOCl_3$. The predecessor to $VOCl_3$ in the gas phase is VOF_3 in the thin film.

The production of S_8 products is much less on the V_2O_5 surface. Vanadium in V_2O_5 is already in the 5+ oxidation state and

Published under an exclusive license by the AVS

can directly produce volatile 5+ oxidation state etch products. Consequently, oxidation of V_2O_5 is not necessary and less reduction of SF_4 to S_8 is required for etching V_2O_5. The V_2O_5 also etched much more rapidly than VO_2. After exposure to six cycles of BCl_3 and SF_4 at 250 °C, the VO_2 powder mass was reduced from 53.8 to 46.6 mg for a 13% mass loss. In comparison, after exposure to five cycles of BCl_3 and SF_4 at 250 °C, the V_2O_5 powder mass was reduced from 23.5 to 1.1 mg for a 95% mass loss. The oxidation state change required for VO_2 etching to produce volatile vanadium etch products in the 5+ oxidation state must limit the rate of VO_2 etching.

Time-resolved QMS results for the volatile etch products during a BCl_3 exposure on V_2O_5 are shown in Fig. 9. V_2O_5 is shown instead of VO_2 because the vanadium etch products are more intense from vanadium in the 5+ oxidation state. However, similar products are also observed for VO_2. Early during the BCl_3 exposure at t = 10 s, Fig. 9(a) shows the ion intensity for $VOCl_3^+$ from the $VOCl_3$ volatile etch product. The electron impact ionization of $VOCl_3$ also leads to $VOCl_2^+$ and VCl_3^+ fragment ion signals.[53]

As the BCl_3 exposure continues at t = 28 s, Fig. 9(b) reveals that the ion intensities for VCl_4^+ and VCl_3^+ become the most significant species. These ion intensities result from electron impact ionization of VCl_4. The appearance of VCl_4 is expected from the conversion of VO_2 to B_2O_3 given by Eq. (1). Later in the exposure at t = 70 s, Fig. 9(c) shows that trichloroboroxin ($B_3O_3Cl_3$) rings become prominent as BCl_3 interacts with the converted B_2O_3 surface. Trichloroboroxin has been observed earlier during etching of B_2O_3 by BCl_3.[33] Small signals for trichloroboroxin were also detected earlier in Fig. 9(b).

Not shown in Fig. 9 are the ion intensities for $BFCl_2$ and BF_2Cl ligand exchange products in the low mass region. The ion intensities for $BFCl_2^+$ and BF_2Cl^+ reach their maximum intensities simultaneously with the maximum intensity for $VOCl_3^+$ in Fig. 9(a). The maximum intensities are 120 mV for $BFCl_2^+$ at *m/z* 102 and 37 mV for BF_2Cl^+ at *m/z* 84.

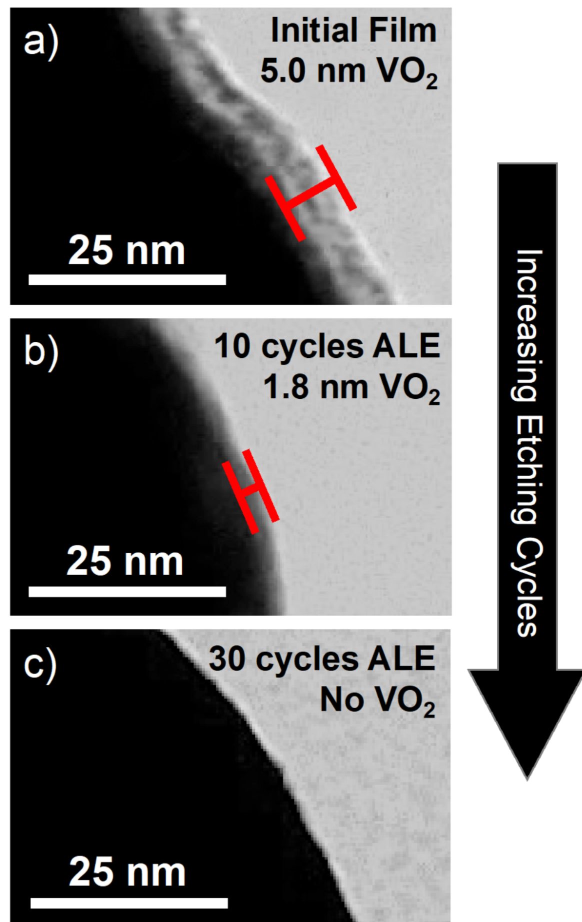

FIG. 10. TEM images of VO_2 ALD films on W particles showing (a) initial VO_2 film with thickness of 5 nm, (b) VO_2 film after 10 VO_2 ALE cycles with a thickness of 1.8 nm, and (c) no remaining VO_2 film after 30 VO_2 ALE cycles.

D. TEM studies

TEM was used to visualize VO_2 ALE on VO_2 ALD films on W particles (10 μm tungsten powder, >99.99%, Sigma-Aldrich). For these experiments, a VO_2 ALD film with a thickness of 5 nm was deposited at 150 °C using 200 VO_2 ALD cycles with TEMAV and H_2O as reactants. The W powders were covered with a native WO_3 surface. The initial quantity of W powder was 1 g. After VO_2 ALD, the sample was removed for the TEM analysis and then placed back into the reactor for VO_2 ALE.

The initial TEM image shown in Fig. 10(a) reveals that the VO_2 ALD film is uniform and conformal on the W particle. The VO_2-coated W powder was then etched using VO_2 ALE at 250 °C. This etching was performed under static etching conditions with 60 s hold times at constant pressure and a purge sequence consisting of 120 s static purging, 240 s viscous N_2 purging, followed by a final 120 s static purge. Reactant pressures were 5 Torr for both BCl_3 and SF_4 exposures. A TEM image was then recorded after 10 VO_2 ALE cycles as displayed in Fig. 10(b). Another TEM image was recorded after 20 additional VO_2 ALE cycles (30 cycles total) as shown in Fig. 10(c).

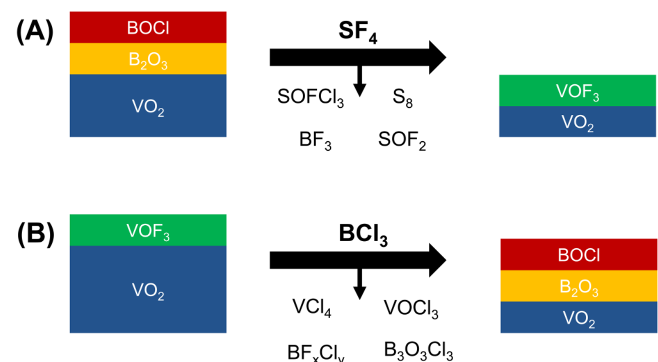

FIG. 11. Schematic of the proposed reaction process for VO_2 ALE showing (a) SF_4 exposure and (b) BCl_3 exposure.

Published under an exclusive license by the AVS

TEM analysis shows that the VO_2 ALD film is progressively removed by VO_2 ALE. The etch rate estimated from the TEM images is ~3.2 Å/cycle at 250 °C. This etch rate is higher than the etch rate of 2.3 Å/cycle at 250 °C measured for the VO_2 ALD films on the QCM sensor. The higher etch rate on the particles is attributed to the static exposures and the lower gas conductance in the VO_2-coated W powder. Similar results are observed during ALD on particles when the ALD growth rates are larger than the growth rates observed on flat surfaces.[54,55]

E. VO_2 ALE reaction mechanism

A proposed reaction mechanism for VO_2 ALE with BCl_3 and SF_4 as reactants is given in Fig. 11. This proposed mechanism attempts to explain all the observations from the QCM, FTIR, and QMS experiments. The key observations were as follows: (1) mass losses observed on both BCl_3 and SF_4 exposures; (2) BCl_3 leading to both conversion of VO_2 to B_2O_3 and BCl_3 acting as a ligand-exchange precursor; (3) sulfur in SF_4 yielding both higher oxidation states in SO_xCl_y volatile species and lower oxidation states in S_8 volatile species; (4) volatile vanadium etch products appearing in both the 4+ oxidation state (VCl_4) and the 5+ oxidation state ($VOCl_3$); and (5) etching of B_2O_3 by BCl_3 to produce $B_3O_3Cl_3$.

Initial reaction equations were written to agree with the surface and volatile species as observed by FTIR and QMS. Mathematica (Wolfram Mathematica 13.0.0.0) was then used to solve the system of many reaction equations to obtain reaction coefficients that agreed with observed QCM mass changes. The balanced reaction equations that are consistent with all the experimental results are given below. In these equations, the * denotes a surface species, the | separates different surface species, and the (g) indicates a gas species.

SF_4 reactions:

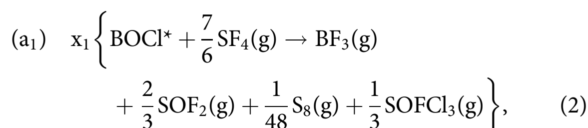

$$(a_1)\quad x_1\left\{BOCl^* + \frac{7}{6}SF_4(g) \rightarrow BF_3(g) + \frac{2}{3}SOF_2(g) + \frac{1}{48}S_8(g) + \frac{1}{3}SOFCl_3(g)\right\}, \tag{2}$$

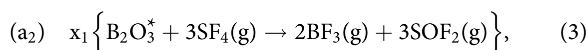

$$(a_2)\quad x_1\left\{B_2O_3^* + 3SF_4(g) \rightarrow 2BF_3(g) + 3SOF_2(g)\right\}, \tag{3}$$

$$(a_3)\quad x_3\left\{VO_2^* + \frac{5}{4}SF_4(g) \rightarrow VOF_3^* + \frac{1}{32}S_8(g) + SOF_2(g)\right\}. \tag{4}$$

BCl_3 reactions:

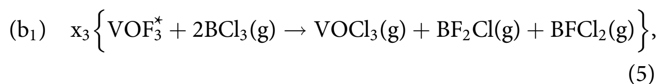

$$(b_1)\quad x_3\left\{VOF_3^* + 2BCl_3(g) \rightarrow VOCl_3(g) + BF_2Cl(g) + BFCl_2(g)\right\}, \tag{5}$$

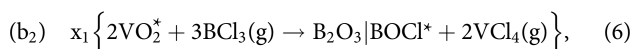

$$(b_2)\quad x_1\left\{2VO_2^* + 3BCl_3(g) \rightarrow B_2O_3|BOCl^* + 2VCl_4(g)\right\}, \tag{6}$$

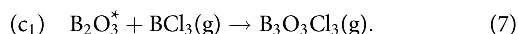

$$(c_1)\quad B_2O_3^* + BCl_3(g) \rightarrow B_3O_3Cl_3(g). \tag{7}$$

The sum of reactions a_1, a_2, and a_3 in Eqs. (2)–(4) presents the overall reaction during the SF_4 exposure. Reaction a_1 in Eq. (2) presents the removal of $BOCl^*$ surface species to produce BF_3, SOF_2, and $SOFCl_3$. Reaction a_2 in Eq. (3) describes the removal of $B_2O_3^*$ surface species to produce BF_3 and SOF_2. Reaction a_3 in Eq. (4) presents the oxidation of VO_2^* to VOF_3^* and the subsequent reduction of SF_4 to S_8. S_8 is produced during reaction a_3 when VO_2 is oxidized to form VOF_3^*. In addition, some S_8 is also produced during reaction a_1 when SF_4 is oxidized to $SOFCl_3$.

The sum of reactions b_1, b_2, and c_1 in Eqs. (5)–(7) gives the overall reaction during the BCl_3 exposure. Reaction b_1 in Eq. (5) describes VOF_3 undergoing a ligand-exchange process with BCl_3 to form volatile $VOCl_3$ and mixed-halogen boron species. Reaction b_2 in Eq. (6) presents the conversion of V_2O_4 (or $2VO_2$) to B_2O_3 and VCl_4. Finally, reaction c_1 in Eq. (7) represents etching of the B_2O_3-converted surface layer during extended BCl_3 exposures to produce trichloroboroxin.

The coefficient values needed to balance the equations and agree with observed QCM mass changes were calculated by Mathematica. See supplementary material[56] for a description of the Mathematica calculations. Mass loss from c_1 was not considered when calculating the reaction coefficients. The Mathematica calculations established that Eqs. (2)–(6) yield the correct ratio of mass changes during SF_4 and BCl_3 exposures with the reaction coefficients $x_1 = 0.82$ and $x_3 = 0.36$.

In addition, the Mathematica calculations determined that the sum of reactions a_1, a_2, and a_3 and the sum of reactions b_1 and b_2 both yield mass losses during SF_4 and BCl_3 exposures, respectively. Mass losses of $\Delta m_{BCl3} = -44.3$ and $\Delta m_{SF4} = -56.9$ ng/cm^2 were measured by QCM at 250 °C for the individual BCl_3 and SF_4 exposures, respectively. The experimental ratio of the mass changes was $\Delta m_{BCl3}/\Delta m_{SF4} = 0.78$. The coefficients x_1 and x_3 for the reaction mechanism given by Eqs. (2)–(6) also produced a ratio of the mass changes of $\Delta m_{BCl3}/\Delta m_{SF4} = 0.78$.

IV. CONCLUSIONS

VO_2 thermal ALE was accomplished using sequential exposures of BCl_3 and SF_4. The etch rates, surface species during etching, and volatile etch products were measured by employing various techniques including QCM, FTIR, and QMS. Using QCM measurements, the VO_2 etch rates varied from 0.05 Å/cycle at 150 °C to 2.3 Å/cycle at 250 °C. Mass losses were observed during both BCl_3 and SF_4 exposures. The mass losses versus BCl_3 and SF_4 exposures were also nearly self-limiting versus BCl_3 and SF_4 exposures. VO_2 ALE was also visualized using TEM studies that observed the removal of VO_2 ALD films on W particles.

FTIR studies were able to observe the surface species and the loss of the VO_2 film during VO_2 thermal ALE. The initial BCl_3 exposures on the VO_2 film were observed to convert the VO_2 to B_2O_3. The subsequent SF_4/BCl_3 reactions led to the growth/loss of absorbance at 1051 and 650 cm^{-1}. These absorbance features were attributed to $F_3V{=}O$ and V—F stretching vibrations, respectively. SF_4 fluorinates VO_2 to form a VOF_3 surface layer and then BCl_3 reacts with VOF_3 by ligand-exchange to volatilize the VOF_3 surface layer as $VOCl_3$. Likewise, BCl_3 also converts some VO_2 to B_2O_3 and then the SF_4 exposure removes the B_2O_3 conversion layer.

The QMS measurements revealed that there were many changes in the oxidation state during VO_2 ALE. SF_4 was oxidized

Published under an exclusive license by the AVS

during SF_4 exposures and various $SO_xF_yCl_z$ products were observed in oxidation states greater than 4+. SF_4 was also reduced all the way to elemental S_8. VCl_4 and $VOCl_3$ were observed as the main vanadium-containing etch products. $VOCl_3$ requires the oxidation of vanadium to the 5+ oxidation state. This oxidation may be coupled with the reduction in SF_4 to produce S_8 species. Trichloroboroxin ($B_3O_3Cl_3$) was also observed during the BCl_3 exposures. $B_3O_3Cl_3$ can be produced after BCl_3 converts VO_2 to B_2O_3 and then proceeds to etch the converted B_2O_3.

Thermal VO_2 ALE using sequential BCl_3 and SF_4 exposures illustrates the variety of surface reactions that can define a thermal ALE process. VO_2 ALE proceeded by many pathways including conversion, ligand-exchange, and oxidation state changes. One factor that adds to the complexity of VO_2 ALE is the potential of BCl_3 for conversion reactions. Another factor is stable and volatile vanadium etch products in the 5+ oxidation state that require oxidation state changes from 4+ in VO_2 to 5+ in $VOCl_3$.

ACKNOWLEDGMENTS

This research was funded by the U.S. Army Research Laboratory and the U.S. Army Research Office under Contract No. W911NF-14-C-0007. The FTIR studies were funded by Intel through a member-specific research grant from the Semiconductor Research Corporation (SRC). Funding for the QMS reactor and the QMS investigations was provided by Lam Research.

AUTHOR DECLARATIONS

Conflict of Interest

The authors have no conflicts to disclose.

Author Contributions

Jonas C. Gertsch: Data curation (lead); Formal analysis (lead); Investigation (lead); Writing – original draft (lead); Writing – review & editing (equal). **Jonathan L. Partridge:** Data curation (supporting); Investigation (supporting). **Austin M. Cano:** Data curation (supporting); Investigation (supporting). **Joel W. Clancey:** Data curation (supporting); Investigation (supporting). **Victor M. Bright:** Conceptualization (equal); Funding acquisition (equal); Project administration (equal); Supervision (equal); Writing – review & editing (supporting). **Steven M. George:** Conceptualization (equal); Funding acquisition (equal); Methodology (lead); Project administration (equal); Supervision (equal); Writing – review & editing (equal).

DATA AVAILABILITY

The data that support the findings of this study are available within the article.

REFERENCES

[1] K. J. Kanarik, T. Lill, E. A. Hudson, S. Sriraman, S. Tan, J. Marks, V. Vahedi, and R. A. Gottscho, J. Vac. Sci. Technol. A **33**, 020802 (2015).
[2] A. Fischer, A. Routzahn, S. M. George, and T. Lill, J. Vac. Sci. Technol. A **39**, 030801 (2021).
[3] S. D. Athavale and D. J. Economou, J. Vac. Sci. Technol. B **14**, 3702 (1996).
[4] S. D. Park, D. H. Lee, and G. Y. Yeom, Electrochem. Solid-State Lett. **8**, C106 (2005).
[5] D. Metzler, R. L. Bruce, S. Engelmann, E. A. Joseph, and G. S. Oehrlein, J. Vac. Sci. Technol. A **32**, 020603 (2014).
[6] S. D. Park, W. S. Lim, B. J. Park, H. C. Lee, J. W. Bae, and G. Y. Yeom, Electrochem. Solid-State Lett. **11**, H71 (2008).
[7] K. S. Min, S. H. Kang, J. K. Kim, Y. I. Jhon, M. S. Jhon, and G. Y. Yeom, Microelectron. Eng. **110**, 457 (2013).
[8] S. D. Park, C. K. Oh, J. W. Bae, G. Y. Yeom, T. W. Kim, J. I. Song, and J. H. Jang, Appl. Phys. Lett. **89**, 043109 (2006).
[9] D. S. Kim, J. E. Kim, W. O. Lee, J. W. Park, Y. J. Gill, B. H. Jeong, and G. Y. Yeom, Plasma Processes Polym. **16**, 1900081 (2019).
[10] W. S. Lim *et al.*, Carbon **50**, 429 (2012).
[11] K. S. Kim *et al.*, ACS Appl. Mater. Interfaces **9**, 11967 (2017).
[12] S. M. George, Acc. Chem. Res. **53**, 1151 (2020).
[13] D. R. Zywotko, J. Faguet, and S. M. George, J. Vac. Sci. Technol. A **36**, 061508 (2018).
[14] A. M. Cano, J. L. Partridge, and S. M. George, Chem. Mater. **34**, 6440 (2022).
[15] Y. Lee, J. W. DuMont, and S. M. George, Chem. Mater. **27**, 3648 (2015).
[16] Y. Lee, J. W. DuMont, and S. M. George, Chem. Mater. **28**, 2994 (2016).
[17] Y. Lee and S. M. George, ACS Nano **9**, 2061 (2015).
[18] Y. Lee, J. W. DuMont, and S. M. George, ESC J. Solid State Sci. Technol. **4**, N5013 (2015).
[19] Y. Lee and S. M. George, J. Vac. Sci. Technol. A **36**, 061504 (2018).
[20] J. A. Murdzek and S. M. George, J. Vac. Sci. Technol. A **38**, 022608 (2020).
[21] Y. Lee, N. R. Johnson, and S. M. George, Chem. Mater. **32**, 5937 (2020).
[22] A. M. Cano, A. Lii-Rosales, and S. M. George, J. Phys. Chem. C **126**, 6990 (2022).
[23] N. R. Johnson, H. Sun, K. Sharma, and S. M. George, J. Vac. Sci. Technol. A **34**, 050603 (2016).
[24] Y. Lee and S. M. George, Chem. Mater. **29**, 8202 (2017).
[25] J. W. DuMont, A. E. Marquardt, A. M. Cano, and S. M. George, ACS Appl. Mater. Interfaces **9**, 10296 (2017).
[26] A. I. Abdulagatov and S. M. George, Chem. Mater. **30**, 8465 (2018).
[27] N. R. Johnson and S. M. George, ACS Appl. Mater. Interfaces **9**, 34435 (2017).
[28] J. A. Murdzek, A. Lii-Rosales, and S. M. George, Chem. Mater. **33**, 9174 (2021).
[29] S. M. George and Y. Lee, ACS Nano **10**, 4889 (2016).
[30] M. Konh, C. He, X. Lin, X. Guo, V. Pallem, R. L. Opila, A. V. Teplyakov, Z. Wang, and B. Yuan, J. Vac. Sci. Technol. A **37**, 021004 (2019).
[31] N. R. Johnson, J. K. Hite, M. A. Mastro, C. R. Eddy, and S. M. George, Appl. Phys. Lett. **114**, 243103 (2019).
[32] P. C. Lemaire and G. N. Parsons, Chem. Mater. **29**, 6653 (2017).
[33] A. M. Cano, S. K. Natarajan, J. L. Partridge, S. D. Elliott, and S. M. George, J. Vac. Sci. Technol. A **40**, 022601 (2022).
[34] J. C. Gertsch, A. M. Cano, V. M. Bright, and S. M. George, Chem. Mater. **31**, 3624 (2019).
[35] HSC Chemistry 9.9.2.3, Outokumpu Research Oy, Pori, Finland.
[36] F. J. Morin, Phys. Rev. Lett. **3**, 34 (1959).
[37] M. Soltani, M. Chaker, E. Haddad, and R. V. Kruzelesky, J. Vac. Sci. Technol. A **24**, 612 (2006).
[38] C. Chen, X. Yi, X. Zhao, and B. Xiong, Sens. Actuators A: Phys. **90**, 212 (2001).
[39] T. D. Manning, I. P. Parkin, M. E. Pemble, D. Sheel, and D. Vernardou, Chem. Mater. **16**, 744 (2004).
[40] J. C. Gertsch, E. Sortino, V. M. Bright, and S. M. George, J. Vac. Sci. Technol. A **39**, 062602 (2021).
[41] T. Blanquart *et al.*, RSC Adv. **3**, 1179 (2013).
[42] G. Rampelberg, D. Deduytsche, B. De Schutter, P. A. Premkumar, M. Toeller, M. Schaekers, K. Martens, I. Radu, and C. Detavernier, Thin Solid Films **550**, 59 (2014).
[43] J. W. DuMont and S. M. George, J. Phys. Chem. C **119**, 14603 (2015).
[44] A. Lii-Rosales, V. L. Johnson, S. Sharma, A. Fischer, T. Lill, and S. M. George, J. Phys. Chem. C **126**, 8287 (2022).

Published under an exclusive license by the AVS

[45]J. W. Clancey, A. S. Cavanagh, J. E. T. Smith, S. Sharma, and S. M. George, J. Phys. Chem. C **124**, 287 (2020).
[46]I. L. Botto, M. B. Vassallo, E. J. Baran, and G. Minelli, Mater. Chem. Phys. **50**, 267 (1997).
[47]I. R. Beattie and T. R. Gilson, J. Chem. Soc. A, 2322 (1969).
[48]R. G. Cavell and H. C. Clark, Inorg. Chem. **3**, 1789 (1964).
[49]H. Selig and H. H. Claassen, J. Chem. Phys. **44**, 1404 (1966).
[50]R. Rulkens, J. L. Male, K. W. Terry, B. Olthof, A. Khodakov, A. T. Bell, E. Iglesia, and T. D. Tilley, Chem. Mater. **11**, 2966 (1999).
[51]D. Peak, G. W. Luther, and D. L. Sparks, Geochim. Cosmochim. Acta **67**, 2551 (2003).
[52]W. B. Maier and R. F. Holland, J. Chem. Phys. **72**, 6661 (1980).
[53]C. F. V. Mason and R. G. Behrens, J. Less-Common Met. **85**, 21 (1982).
[54]J. D. Ferguson, A. W. Weimer, and S. M. George, Thin Solid Films **371**, 95 (2000).
[55]J. A. McCormick, K. P. Rice, D. F. Paul, A. W. Weimer, and S. M. George, Chem. Vap. Depos. **13**, 491 (2007).
[56]See the supplementary material at https://www.scitation.org/doi/suppl/10.1116/6.0002149 for the calculations used to determine the reaction coefficients for the SF4 and BCl3 reactions during VO_2 thermal ALE.

Published under an exclusive license by the AVS